Energy Advances

ROYAL SOCIETY OF CHEMISTRY

PAPER

View Article Online
View Journal | View Issue

Cite this: *Energy Adv.*, 2023, 2, 513

The influence of trinuclear complexes on light-induced hydrogen production†‡

Helena Roithmeyer,[a] Richard Pehn,[a] Johann Pann,[a] Wolfgang Viertl,[a] Benedikt Trübenbacher,[a] Julian Dutzler,[a] Holger Kopacka,[a] Thomas Müller[b] and Peter Brüggeller*[a]

Inspired by nature, artificial molecular systems are designed to produce hydrogen for chemical storage or as a primary source of energy. A class of new trinuclear complex based on a PNP-ligand **3** was synthesised, characterised and investigated for light-induced hydrogen production. To demonstrate the influence of multiple metal centres on the chromophoric and catalytic behaviour, the ability of the systems to produce hydrogen was investigated under various conditions. We found that multiple metal centres hinder each other in the case of chromophores and support each other in the case of WRCs (water reduction catalysts), which was apparent in the form of the received TON (turnover number). UV/Vis spectroscopy and photophysical measurements were conducted to gain insights into the light-induced transitions of the excited chromophoric units. A full photophysical characterisation of the trinuclear chromophore [(Cu(phenanthrolinederivate))$_3$(1,3,5-tris(PNP-Me)-benzene)](PF$_6$)$_3$ (**4d**) is presented and the hydrogen evolution ability was tested when combined with the literature-known and benchmarked catalysts **1** [Ni(py-S)$_3$](NEt$_4$) and **2** [Fe$_3$(CO)$_{12}$]. Trimetallic WRCs based on Pd, Pt, Co, Ni, and Fe were developed and the ability of the non-noble and noble metal-based systems to produce hydrogen was studied. Different sunlight imitating light sources were used to optimise the final TON and turnover frequency (TOF). Additionally, the redox states of the most promising WRCs were analysed by cyclic voltammetry (CV) to gather information about their water reduction ability. A major preparative effort has been undertaken in order to obtain at least some excellent chromophores and/or WRCs. For the trinuclear chromophore **4d**, only a modest TON of 48 could be achieved. However, the trinuclear WRC [(Pd(ACN)$_2$)$_3$(tris(PNP-Me)benzene)](PF$_6$)$_6$ (**8b**) showed excellent TONs up to 8899 and a turnover frequency (TOF) of 2737 h^{-1} with a correlating incident photon conversion efficiency (IPCE) of 2.1%. These values are among the best regarding molecular WRCs. The structurally similar non-noble metal-based WRCs with iron and nickel showed TONs of 290 and 460, respectively.

Received 8th January 2023,
Accepted 8th February 2023

DOI: 10.1039/d3ya00015j

rsc.li/energy-advances

A Introduction

The demand for storable and environmentally friendly energy sources to replace hydrocarbon-based fuels has gained extensive attention in the last decade. The continuous decrease in fossil fuels as well as the economic and population growth require alternative energy sources.[1,2] Artificial systems, inspired by natural photosynthesis, were designed to convert light energy into chemical energy and were studied for their hydrogen production ability.[3–6] Light-induced water splitting based on the concept of molecular artificial photosynthesis (AP), consisting of a photosensitiser (PS), a water reducing catalyst (WRC) and a sacrificial donor, which first reduces the PS as a consequence of its excess, is applied with the designed systems.

A special phosphine ligand was invented to stabilise WRCs[5,7–10] during catalysis and to increase the rigidity of the ligand backbone for chromophores.[11–13] The electronic and steric effects of the substituents on the phosphine ligand have an influence on the auxiliary ligands and their transition metal complexes: electronegative substituents lower the energy gap of the anti-binding σ*-orbitals, benefitting π-acceptor properties.[14,15] In this work, the newly developed tris-ligand (Scheme 1, **3**) is substituted with methoxy groups in the *ortho* positions of the

[a] *Centrum for Chemistry and Biomedicine, Institute of General, Inorganic and Theoretical Chemistry, University of Innsbruck, Innrain 82, 6020 Innsbruck, Austria. E-mail: Peter.Brueggeller@uibk.ac.at; Tel: +43 664 3461922*
[b] *Centrum for Chemistry and Biomedicine, Institute of Organic Chemistry, University of Innsbruck, Innrain 82, 6020 Innsbruck, Austria*

† Electronic supplementary information (ESI) available. CCDC 2110798 (**4d**). For ESI and crystallographic data in CIF or other electronic format see DOI: https://doi.org/10.1039/d3ya00015j

‡ The obtained data were taken from the dissertation of Helena Roithmeyer, LFU Innsbruck, July 2020 and from the dissertation of Johann Pann, LFU Innsbruck, 2022.

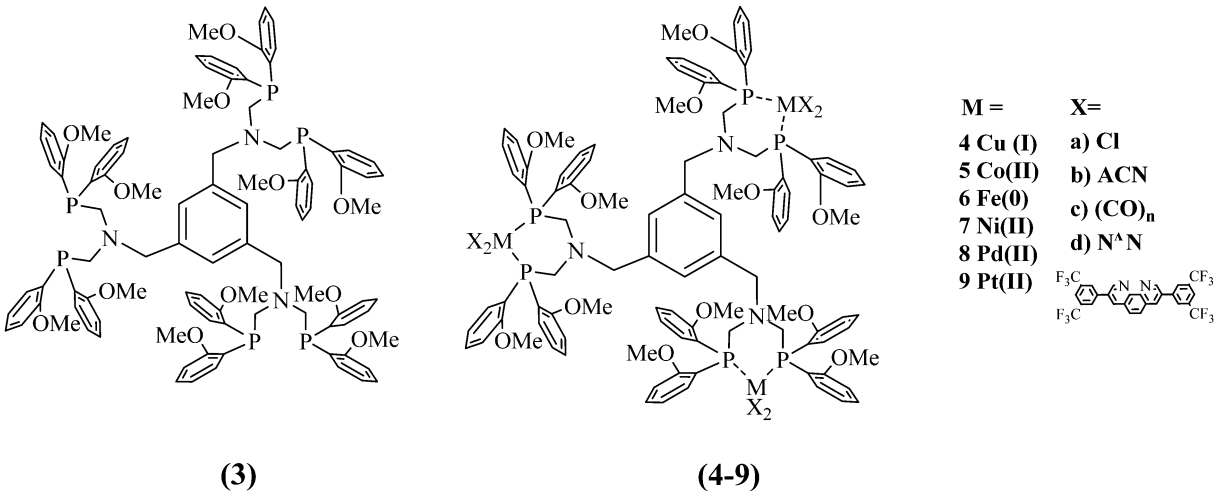

Scheme 1 The 1,3,5-Tris(PNP-Me)benzene (**3**) ligand and complexed forms (**4–9**).

phenyl residues at the P atoms, which causes an inductive electron withdrawing effect and is stabilised through mesomerism. Moreover, anisyl phosphines exhibit enhanced catalytic stability compared to phenyl phosphine analogues.[5,6,15,16] Another beneficial preparative side effect is that the educt di-*ortho* anisyl phosphine is a powder and easy to handle in comparison to its easily inflammable diphenyl phosphine relative, which makes it attractive for larger scale reactions. Similar systems of the mono- and bis-ligand with phenyl instead of anisyl groups already exist.[6,15,17–21]

In this study, we present, to the best of our knowledge, for the first time, an anisyl containing PNP-ligand with multiple coordination sites to produce trimetallic complexes. Their mononuclear relatives do not exhibit the benzene function.[19,22–24] The size of the ligand sphere directly influences the reactivity of the attached metal centre and, therefore, subsequent catalysis. Bulky ligands influence bond distances as well as steric compression.[23] Inserted proton relays in the form of an amine function are intended to facilitate proton binding, proton transfer and hydride binding to the catalytic metal centre.[9,25–27]

It has also been reported that pendant amines support rapid hydride formation and proton–hydride coupling in the immediate vicinity of the metal centres, leading to increased hydrogen formation rates. Beyond that, it is assumed that the basicity of the neighbouring amines in interaction with the hydride acceptor capability of the metal centre favours thermodynamically favourable processes, which leads to higher and faster hydrogen evolution.[25,26,28–32] The newly synthesised 1,3,5-tris(PNP-Me)benzene (tris, **3**) ligand exhibits three possible coordination sites all equipped with proton relays.

The use of anisyl groups in the ligand is expected to lead to more stable, and longer-lived metal-to-ligand charge transfer (MLCT) states after excitation, rendering them as suitable ligands for PS. The charge separation and the sufficient electron transfer thus favour the water reduction, which is promoted by the light absorption of the chromophore.[15] For N_2–Cu(I)–N_2 ligands, it was reported that the absorption of a photon leads to a Cu(II)* excited state surrounded by a reduced and neutral N-ligand. The formal oxidation to Cu(II) leads to an electron transfer to one N-ligand, generating a Franck–Condon MLCT state. As a result, a Jahn–Teller distortion leads to a flattening of the tetrahedral coordination, implying a geometry change, which is usually known for Cu(II) complexes.[17,32–35] The Cu(I) flattening is suppressed by sterically demanding phosphine or phenanthroline ligands.[33,36–43] In particular, flexible linking systems affect electron transfer and may result in geometry alteration. Aromatic bridges show higher catalytic rate constants than aliphatic systems.[44–48] The trinuclear complex **4d** of the form $(P_2Cu(I)N_2)_3$ was synthesised and investigated for its catalytically relevant photophysical behaviour during light exposure, and the resulting chromophoric behaviour is discussed. The trinuclear chromophore was combined with the literature-known and benchmarked catalysts $[Ni(py\text{-}S)_3](NEt_4)$ (**1**) and $[Fe_3(CO)_{12}]$ (**2**). Different non-noble and noble metals were implemented with the newly developed ligand **3** to form suitable water reduction catalysts **5–9** and their activity and performance combined with the literature-known chromophore $[Ir(bpy)(ppy)_2](PF_6)$ was tested under different irradiation conditions to shed light on the benefit of multiple active sites.

B Syntheses and characterisation

A new PNP-ligand with three possible coordination sites (Scheme 1, **3**) was synthesised to enable the coordination of multiple catalytic active metal centres (Scheme 1, **4–9**). The synthesis and characterisation of the tris ligand can be found in the ESI† (^{1}H and ^{31}P NMR, ESI-MS, elemental analyses). To determine the viability of ligand **3** for multinuclear PSs or WRCs, different metals were coordinated and investigated. First ligand **3** was coordinated to Cu(I) and a bulky phenanthroline derivate (Scheme 1, **4d**) and the influence of multiple chromophoric metal centres on the photophysical properties was studied. The complex **4d** was tested for its hydrogen production ability when inserted with different literature-known WRCs. The idea was to create a more sustainable catalytic system consisting of a

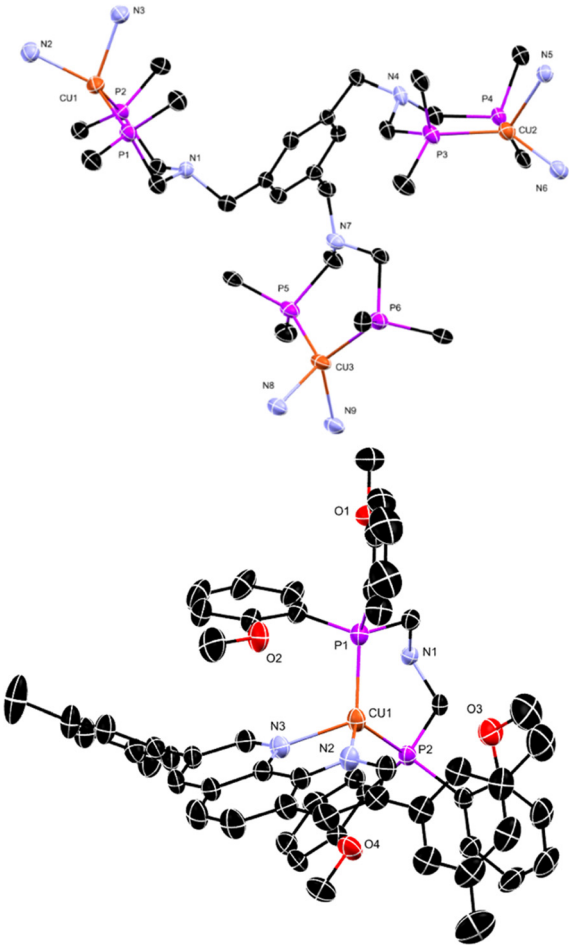

Fig. 1 Crystal structure of [(Cu(3,8-bis[3,5-bis(trifluoromethyl)phenyl]-1,10-phenanthroline)$_3$(1,3,5-tris(PNP-methylene)benzene)](BF$_4$)$_3$, **4d**. Anions, solvent molecules, and protons are omitted for clarity. Above: only the pivot atoms of the anisyl groups and the 3,5-bis(trifluoromethyl)phenyl]-1,10-phenanthroline ligands are shown. Below: the steric crowding around the Cu1 centre is shown. The Cu1···O2, Cu1···O3, and Cu1···O4 contact distances are 3.391, 3.423, and 3.358 Å, respectively. O1 is orientated away from the Cu1 centre. Only the carbon pivot atoms of the CF$_3$ groups are depicted.

Cu(I) PS and a non-noble metal based WRC containing nickel or iron. For more detailed information about the synthesis and the characterisation, see the ESI† (Scheme S3). In order to characterise one example of the complexes containing the new ligand completely (Fig. 1 and Table 1), single crystals suitable for an X-ray structure analysis with the composition $C_{183}H_{141}B_3Cu_3F_{48}N_9O_{12}P_6$·0.95diethylether·2water·0.86acetonitrile were obtained by gas phase diffusion of diethyl ether into an acetonitrile solution of **4d** in its BF_4^--form. Water molecules have been incorporated into the lattice.

Different WRCs were developed and synthesised according to Scheme S4, ESI.† Except for the platinum(II) complex **9b**, the different tris-complexes were obtained in high yields: **4d** 84%, **5a** 46%, **6c** 74%, **7a** 79%, **7b** 98%, **8a** 62%, **8b** 60%, and **9b** 14%. Lower yields can be explained by the larger size of the corresponding metals which disfavour coordination with the bulky ligand. Anion exchange was obtained by adding an excess of TIPF$_6$ to the chlorido complexes in MeCN. Detailed synthesis strategies and characterisation for each complex **4–9** can be found in the ESI.†

Table 1 Crystallographic data, selected bond distances [Å] and bond angles [°] of **4d**

a	25.6400(3) Å	Unique reflections	30 193
b	19.3584(2) Å	D_x	1.339 g cm^{-3}
c	41.4109(5) Å	M_r	4115.92
β	96.7070(6)°	Z	4
V	20413.6(4) Å^3	S	1.021
Crystal system	monoclinic	R_1 (all data)	0.0782
Space group	$P2_1/c$	R_1 ($I > 2\sigma(I)$)	0.0497
T	173 K	wR_2 (all data)	0.1255
Wavelength	0.71073 Å	wR_2 ($I > 2\sigma(I)$)	0.1127
Cu1–P1	2.195(1)	P1–Cu1–P2	105.80(4)
Cu1–P2	2.203(1)	N2–Cu1–N3	82.36(11)
Cu2–P3	2.2028(9)	N2–Cu1–P1	127.84(9)
Cu2–P4	2.2049(9)	N3–Cu1–P2	109.57(8)
Cu3–P5	2.217(1)	P3–Cu2–P4	102.34(3)
Cu3–P6	2.229(1)	N5–Cu2–N6	81.47(10)
Cu1–N2	2.011(3)	N5–Cu2–P4	109.71(7)
Cu1–N3	2.070(3)	N6–Cu2–P3	120.85(8)
Cu2–N5	2.095(3)	P5–Cu3–P6	104.76(3)
Cu2–N6	2.006(3)	N8–Cu3–N9	82.04(11)
Cu3–N8	2.066(3)	N8–Cu3–P5	121.73(8)
Cu3–N9	2.041(3)	N9–Cu3–P6	123.03(8)

C Results and discussion

The single crystal X-ray structure of **4d** is given in Fig. 1. Table 1 contains the crystallographic data and selected bond distances and bond angles. **4d** shows three distorted tetrahedral Cu(I) centres (Fig. 1 above). The distortions are mainly a consequence of the small N–Cu–N chelate angles of 82.36(11), 81.47(10), and 82.04(11)°, respectively. Interestingly, the Cu(I) centres are sterically shielded by the methoxy groups (see Fig. 1 below). In the case of Cu1, the corresponding contact distances are 3.391, 3.423, and 3.358 Å, respectively. For Cu2 and Cu3, comparable contact approaches occur. Shielding of Cu(I) centres is important in order to prevent the deactivation of MLCT states by interaction and coordination of solvent molecules.

To evaluate the photophysical transition of **4d** during exposure to light and to study the influence of multiple active chromophoric units, the optical properties of the synthesised complex **4d** were studied using UV/Vis-spectroscopy. Photophysical measurements of the lifetimes and emission at different temperatures determine the chromophoric properties and the influence on hydrogen production. The complex exhibits an absorption maximum of 280 nm, and its metal to ligand charge transfer absorption can be found at 480 nm (Fig. S1a, ESI†). Multiple excitation steps occur, which is apparent in the form of multiple absorption maxima. The –CF$_3$ groups in the fluoro phenanthroline contribute to the red shift of the absorption maxima, showing an electron withdrawing effect, thus lowering the energy of the MLCT states[49] comparable to phenanthroline ligands with enlarged π-systems, which also contribute to a bathochromic shift of the MLCTs. To determine the behaviour of the sterically hindered PS **4d**, photophysical investigations

were conducted, and the result is depicted in Fig. S1b (ESI†) and summarised in Table S1 (ESI†). Surprisingly, the complex **4d** demonstrated weak emission in solution at RT and 77 K, where lifetimes in the nanosecond range were observed. The emission maximum appeared at 688 nm at RT. A large non-radiative decay rate was recognised for compound **4d**, which is assumed to be caused by the multiple metal centres facilitating additional non-radiative energy transfer decay channels. These observations suggested that the Cu(I) centres interfere among themselves. During stimulation, an excited electron is transferred to a nearby metal or ligand, which can hamper the transfer to the WRC. It was noteworthy that several excited chromophore centres negatively affect each other and hinder electron transfer to the catalytic centre. These results led to our assumption that multiple metal centres could be more beneficial when inserted as WRCs. Therefore, we designed different noble and non-noble metal based WRCs (Scheme 1, compounds **5–9**) with the newly designed ligand **3** and compared their catalytic performance in combination with the well-studied and literature known PS $[Ir(bpy)(ppy)_2](PF_6)$. The thermodynamic and mechanistic aspects of the photocatalytic activity of the WRCs presented in this paper have been studied in detail for their mononuclear analogues by DFT calculations.[6] Two-step reductions of the WRCs by the reduced chromophores are followed by oxidative addition of two protons and finally by the release of dihydrogen, thus closing the catalytic cycle. It has been shown that the presence of proton relays has a major impact on the activity of the WRCs.

Hydrogen production capability was examined *via* irradiation studies using the chromophores and WRCs presented above. Regarding the performance of the WRCs, all TON values have been obtained by at least double measurements, whereas in the case of isotope effects also different methods have been used (see ESI,† page 11). The maximal relative standard deviation has been carefully determined to be 1.5% (see ref. 6). Different conditions, such as irradiation intensity and source or molar ratios of the employed compounds, were studied (Tables 2–4). The used irradiation equipment, solutions and flasks are listed in Tables S2–S4 (ESI†). The hydrogen content (ppm) was measured with a GC and is given in terms of the turnover number (TON). In the following tables, figures and discussion, the 1,3,5-tris(PNP-Me)benzene ligand is abbreviated as "tris" and the WRCs as "tris$(MX_2)_3$". Thereby, M describes the coordinated metals and X the complexed ligands at the catalytically active sites.

The PS **4d** was tested during exposure to light using the well-known non-noble metal based WRCs $[Ni(py\text{-}S)_3](NEt_4)$ (**1**) and $[Fe_3(CO)_{12}]$ (**2**). The conditions and results of the experiments are shown in Fig. S7 (ESI†) and listed in Table 2. Different intensities of the irradiation sources and WRC ratios were chosen in order to obtain the best catalytic results. A similar activity was observable for both lamps resulting in a hydrogen evolution of **4d** of up to 40 h. When inserting **4d** with two different WRCs, it was noteworthy that the combination with **1** as a WRC led to higher TONs than with the catalyst **2**. The highest TON value (48) for **4d** in combination with the WRC **1** was recorded after 40 h. The TON of the Cu/Fe based system was increased to 37 (Table 2, entry 3) by the prolongation of the irradiation time (95 h) and an increased solvent volume (325 mL). The catalysts were also measured without the chromophores, where no significant H_2 production was detected, to ensure the dependence of the hydrogen production on the developed chromophores (see ESI,† page 18). Conclusively, it can be noticed that the Cu(I) flattening is restricted by the coordination of bulkier phenanthroline ligands, causing higher TONs due to the suppression of non-radiative decays in the excited state. This makes **4d** the best chromophore, where analogous complexes with neocuproine or bathocuproine show weaker catalytic results. However, from our obtained data, we assume that multiple chromophoric metal centres are prone to energy transfer and may hinder sufficient electron transfer to the catalyst, resulting in overall low TONs. Similar non-noble-metal based mononuclear systems were reported to exhibit TONs up to 1130,[50,51] which strengthened our assumption that multiple chromophoric centres within one system are contra-productive. Therefore, a more promising approach could be the insertion of the molecular trinuclear copper catalysts in the form of a rigid MOF[52] system as a water oxidation catalyst[53,54] or for CO_2 reduction.[55] However, preliminary investigations with cyclic voltammetry showed promising catalytic behaviour of the newly designed multinuclear WRCs. This is why we decided to focus on inserting ligand **3** to obtain optimised and phosphine-stabilised WRCs. This turned out to produce excellent catalytic results (*vide infra*). A criterion to evaluate the production of hydrogen dependent on the amount of water is the oxidation state of the metal centre. Therefore, CV analysis was performed to provide electrochemical information on the most promising WRC during catalysis. The CV analysis of **8b** and with the addition of a defined amount of water is shown in Fig. 2. The resulting cyclic voltammogram recorded the reduction of the palladium(II) centre at a potential of −1.5 V. The presence of an excess of water resulted in a more positive potential. A catalytic wave at −2 V pointed to the reduction of the overpotential in the presence of more water, which indicates that the compound is a highly effective WRC. The CV with 30 μl water looks very different to the others because this is typical for the presence of a low amount of substrate, where the catalytic wave is only in the beginning. For the CVs with higher water contents and below −1.8 V, the onset of the plateau current can be clearly seen. The CV of the non-coordinated tris ligand **3**, which is irreversibly oxidised, can be found in the ESI† (Fig. S2a). Catalysts are known to reduce

Table 2 Irradiation conditions of **4d** and the inserted WRCs $[Fe_3(CO)_{12}]$ (**1**) or $[Ni(py\text{-}S)_3](NEt_4)$ (**2**)

Entry	PS	WRC	*n*PS (μmol)	*V* (mL)	Time (h)	H_2 (ppm)	TON_{PS}	TON_{WRC}
1	**4d**	$[Ni(py\text{-}S)_3](NEt_4)$	0.24	17	21	15 126	48	3
2	**4d**	$[Fe_3(CO)_{12}]$	0.49	19.5	41.5	9327	16	0.8
3	**4d**	$[Fe_3(CO)_{12}]$	0.31	325	95	791	37	1.8

Conditions: $[Fe_3(CO)_{12}]$: T = 23 °C, Solution 1, lamp 3; Schlenk A; ratio PS : WRC 1 : 20 (best ratio for this catalytic system); $[Ni(py\text{-}S)_3](NEt_4)$: T = 23 °C, solution 2, lamp 1, Schlenk A; ratio PS : WRC 1 : 10 (best ratio for this catalytic system). $V = V_{Schlenk} - V_{solution}$.

Table 3 TONs and irradiation conditions of the tris-WRCs with 700 W irradiation

Entry	PS	WRC	*n*WRC (μmol)	*V* (mL)	Time (h)	H_2 (ppm)	TON_{WRC}	TON_{PS}
1	$[Ir(bpy)(ppy)_2](PF_6)$	**9a** $tris(PtCl_2)_3$	0.40	335	233	29 652	1114	93
2	$[Ir(bpy)(ppy)_2](PF_6)$	**8a** $tris(PdCl_2)_3$	0.45	340	233	151 140	5154	429
3	$[Ir(bpy)(ppy)_2](PF_6)$	**8a/b** $tris(PdCl_2)_2(PdACN_2)$	0.32	325	233	70 736	3332	277
4	$[Ir(bpy)(ppy)_2](PF_6)$	**8b** $tris(PdACN_2)_3$	0.28	355	277	233 646	8899	742
5	$[Ir(bpy)(ppy)_2](PF_6)$	**7a** $tris(NiCl_2)_3$	0.58	355	277	16825	460	38
6	$[Ir(bpy)(ppy)_2](PF_6)$	**6c** $tris(Fe_3(CO)_{11})$	0.53	325	277	10 604	291	24
7	$[Ir(bpy)(ppy)_2](PF_6)$	Reference	2.90	320	48	197	—	2.6

Conditions: RT, 15 mL irradiation solution 2, lamp 2, Schlenk B, ratio PS : WRC 12 : 1. $V = V_{Schlenk} - V_{solution}$.

Table 4 TONs and irradiation conditions of tris-WRCs **5**, **7**, and **8** with Solar Light Lab Luminaire LED irradiation

Entry	PS	WRC	*n*WRC (μmol)	*V* (mL)	Conditions	Time (min)	H_2 (ppm)	TON_{WRC}	TON_{PS}
1	$[Ir(bpy)(ppy)_2](PF_6)$	**7a** $tris(NiCl_2)_3$	0.47	156	100 mW, Schlenk B Ratio PS : WRC 6 : 1	460	3956	53	8.8
2	$[Ir(bpy)(ppy)_2](PF_6)$	**7b** $tris(NiACN_2)_3$	0.47	146	100 mW, Schlenk B Ratio PS : WRC 6 : 1	460	4720	59	9.8
3	$[Ir(bpy)(ppy)_2](PF_6)$	**8a** $tris(PdCl_2)_3$	0.29	330	515 nm, 100 mW Schlenk B Ratio PS : WRC 6 : 1	180	25 355	1291	215
4	$[Ir(bpy)(ppy)_2](PF_6)$	**8a** $tris(PdCl_2)_3$	0.31	325	180 mW, Schlenk B Ratio PS : WRC 12 : 1	140	74 774	3482	290
5	$[Ir(bpy)(ppy)_2](PF_6)$	**8b** $tris(PdACN_2)_3$	0.38	355	180 mW, Schlenk B Ratio PS : WRC 12 : 1	335	13 4724	5605	467
6	$[Ir(bpy)(ppy)_2](PF_6)$	**8b** $tris(PdACN_2)_3$	0.38	325	100 mW, Schlenk B Ratio PS : WRC 12 : 1	260	136 682	5206	72
7	$[Ir(bpy)(ppy)_2](PF_6)$	**5a** $tris(CoCl_2)_3$	0.47	157	100 mW, Schlenk B Ratio PS : WRC 6 : 1	460	10 843	146	24
8	Blank $[Ir(bpy)(ppy)_2](PF_6)$	—	0.76	355	100 mW, Schlenk B	70	215	—	0.3

The irradiation solution is warmed up during the irradiation period to T = 35–45 °C after 5 to 15 minutes of irradiation with the 100 mW LED and T = 45–55 °C with the 180 mW LED at 470 nm. Conditions if not stated otherwise: 15 mL irradiation solution 2; lamp 3, 470 nm. An $[Ir(bpy)(ppy)_2](PF_6)$ reference (entry 8) was measured to guarantee that the hydrogen evolution is dependent on the WRCs.

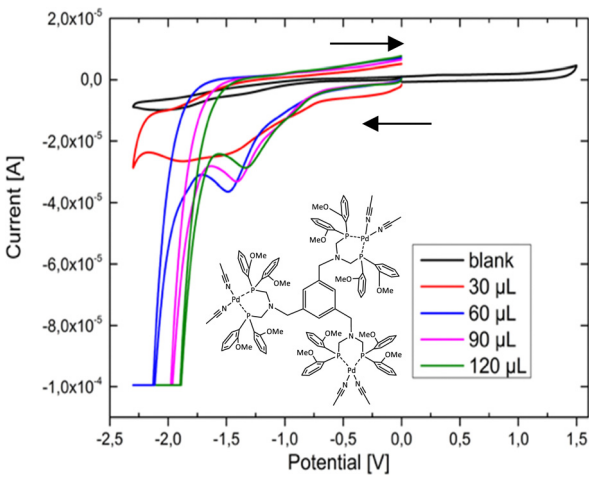

Fig. 2 Cyclic voltammogram of **8b** at different water concentrations. Dry MeCN as solvent, electrodes: WE: glassy carbon GC, RE: $Ag/AgNO_3$, CE: Pt (PF_6 is omitted for clarity in the figure).

the hydrogen overpotential, causing an enhancement of the hydrogen discharging rate. Catalytic waves occur at less negative potentials in comparison to the usually observed hydrogen discharge waves and are a special type of kinetic wave.[56,57]

The non-noble metal-based WRC **7a** was examined in a similar experiment (CVs, Fig. S2b, ESI†), showing an identical effect as **8b**.

To evaluate the behaviour of the multinuclear WRCs during water reduction, different irradiation experiments were carried out. First, the trinuclear WRCs were investigated for their hydrogen production ability using different irradiation sources to achieve optimised conditions for the WRCs. In order to rule out the possibility of colloidal metal formation, a drop of mercury was added to several test solutions resulting in only a slight decrease in catalyst activity. Furthermore, DLS experiments on clear solutions of **8a** or **8b** during irradiation did not show any presence of colloidal particles. However, at the end of the irradiation experiments, small amounts of palladium black could be observed, indicating that as soon as the molecular catalysts are destroyed, the photochemical production of hydrogen stopped. When monitoring the irradiation mixtures after irradiation with ^1H and ^{31}P NMR, decomposition of the complexes and phosphine oxidation was observable. Moreover, black particles formed over time, which could indicate the precipitation of the metals(0), confirming the lack of stabilisation of any palladium colloids and also as a consequence of the absence of any coagulation protecting agent. Therefore, we suggest that the catalytic activity is restricted to the irreversible decomposition of the compounds and we terminated the

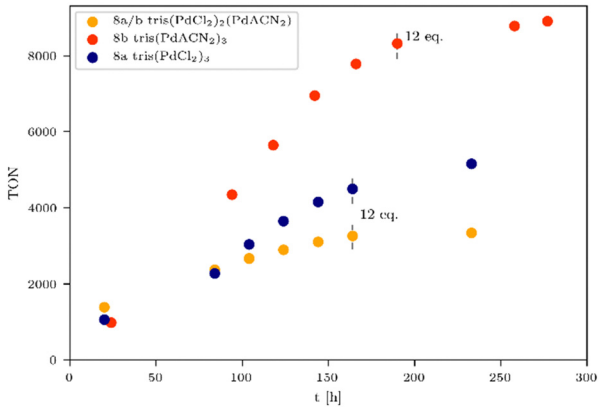

Fig. 3 TONs of palladium based tris-WRCs **8a–b**. During the long-term irradiation (700 mW Hg lamp), two equivalents of chromophore were added at every measurement point, until a total amount of 12 equiv., marked with a line. The mixture of tris($PdCl_2$)$_2$($PdACN_2$) **8a/b** (yellow), in which the chloride was only partially substituted against ACN, displayed a lower TON of 3332 than the pure **8b** with 8899.

irradiation experiments individually when no further hydrogen evolution was detected.

A long term irradiation with a 700 W Hg medium pressure lamp (Table S3, entry 2, ESI†) allowed the irradiation of the tris-WRCs **5–9** for up to nearly 300 h with maintained stability and constant hydrogen evolution. The highest hydrogen production was achieved with the palladium based WRCs **8a–b** (Fig. 3 and Table 3, entries 2–4). The best result was shown for the tris($PdACN_2$)$_3$ **8b**. Due to the ligand exchange (ACN *vs.* Cl), the hydrogen evolution could be enhanced from **8a** TON = 5154 (Fig. 3, blue) to **8b** TON = 8899 (Fig. 3, red).

Table 3 clearly indicates that the catalytic activity is dramatically reduced as soon as the metals present in the WRCs change from 4d to 3d. This is certainly a consequence of a stability problem regarding the 3d WRCs and is typical for this kind of catalysis. It is a major challenge to replace expensive 4d with inexpensive 3d elements. Surprisingly, the platinum-based WRC **9a** (Table 3, entry 1 and Fig. 4, green) showed lower hydrogen production (TON = 1114) than the palladium-based WRCs, where also **9b** shows no improvement. They are therefore compared with the non-noble metal-based WRCs **6c** and **7a** (Fig. 4), which reached a TON of 460 for **7a** tris($NiCl_2$)$_3$ (Fig. 4, pink) and 291 for **6c** tris($Fe_3(CO)_{11}$)$_3$ (Fig. 4, purple).

To influence the turnover frequency (TOF) of the hydrogen formation, a more focused light source was used. The irradiation with a specially developed LED system from the company Bartenbach (Solar Light Lab Luminaire, Table S3, entry 3) (for more information see ESI,† pages 11–16) favours fast hydrogen evolution, and therefore, the turnover frequency (TOF) of the most promising systems was determined. In the following, the catalytic activity of non-noble and noble metal-based WRCs is compared, and the results of the experiments are listed in Table 4. It was noteworthy that anionic exchange led to an increased hydrogen formation within all investigated systems in Fig. 3, 5, and 6. The chlorinated tris($NiCl_2$)$_3$ **7a** is less active than the solvato-complex tris($NiACN_2$)$_3$ **7b** (Fig. 5, blue *vs.* red and Table 4, entries 1 *vs.* 2). This is the same effect as observed for complexes **8a** and **8b**. Under these LED conditions, anion exchange of chloride against ACN caused a higher TON (5605, Table 4, entry 5) in comparison to the chlorinated compound (TON 3482, Table 4, entry 4). To evaluate the most active non-noble metal-based system, the trinuclear catalysts were irradiated with the same irradiation source (Table S3, lamp 3, ESI†) and amount of chromophore (Fig. 5). We found that the tris($CoCl_2$)$_3$ **5a** showed the highest hydrogen production of all investigated non-noble metal-based compounds with a related TON of 146 (Fig. 5, orange and Table 4, entry 7).

The most promising WRCs **8a** and **8b** were irradiated with a higher intensity (180 mW) LED system to study the influence of the irradiation source on the turnover frequency (TOF) and final TON (Fig. 6). Here, it is important to mention that an increase of hydrogen formation with multinuclear catalysts was observed in all experiments, and the optimised conditions for each WRC such as irradiation source, intensity, wavelength and time, play an immense role for the catalytic activity and

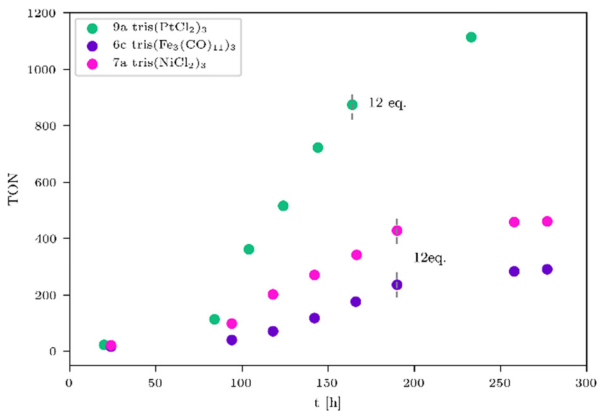

Fig. 4 TONs of different tris-WRCs **6c**, **7a**, and **9a**. During long-term irradiation (700 mW Hg lamp), two equivalents of chromophore were added at every measurement point, until a total amount of 12 equiv., marked with a line.

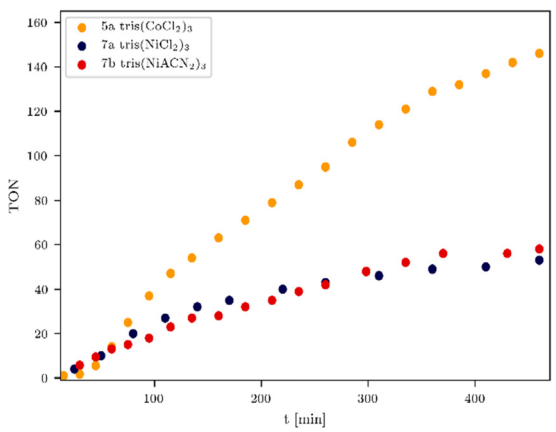

Fig. 5 TONs of non-noble metal based WRCs **5a**, **7a** and **7b**. Conditions: 180 mW, 470 nm, 6 equiv. chromophore.

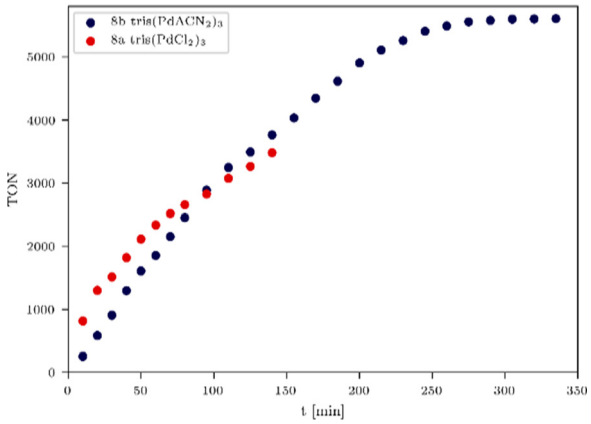

Fig. 6 TON comparison of tris($PdCl_2$)$_3$ **8a** (red) and tris($PdACN_2$)$_3$ **8b** (blue) with 12 equiv. of PS, 470 nm, 180 mW LED irradiation.

endurance. Multinuclear WRCs do increase the final TON as long as access to the catalytic centres is sufficiently provided. In order to screen the most suitable conditions for our developed WRCs, different intensities and chromophore addition points were investigated. We found that higher irradiation intensities caused an increase of the TON of all systems, where the most promising WRC **8b** (Table 4, entry 5) exhibited again the highest TON (5605) of all investigated systems under these conditions.

Moreover, the addition of chromophore in 2 equiv. steps up to 12.0 equiv. at each measuring point led to an acceleration of the hydrogen evolution and thus to a faster increase of the TON, which ended after 260 min irradiation (Fig. 6). A turnover frequency (TOF) was calculated to provide information about how fast a catalyst produces hydrogen. For this experiment (Table 4, entry 5), a TOF of 2737 h^{-1} (Fig. 6, blue) was calculated, and the resulting incident photon conversion efficiency (IPCE, see ESI†) for trimetallic **8b** is 2.1%. In order to make this calculation of the IPCE possible, a calibration of the photoreactor by actinometry has been performed (see the ESI,† pages 12–17).

At this point, we want to highlight that our newly designed systems can reach not only high TON but also fast hydrogen production and high IPCEs considering molecular systems. Moreover, the inserted amount of WRCs is extremely low (<1 μmol), which makes them attractive WRCs. A control experiment with D_2O instead of H_2O shed light on the catalytic cycle and kinetics of the hydrogen evolution reaction and demonstrated that the protons are provided from water during catalysis (for further information, see the ESI,† Fig. S3). When comparing our systems to literature values, we found that our multinuclear PS is not exceeding the reported values for a similar Cu/Fe based system.[50,51] However, our newly developed multinuclear WRCs showed promising results. Even though highly efficient Co and Ni-based electrocatalysts were reported in recent years,[58,59] high TONs based on photocatalytic water splitting with non-noble metal-based WRCs are rare, and since the conditions vary strongly in the different research groups only examples with the same PS are brought below. For example, a mononuclear Co-based WRC combined with the same iridium PS as in our work reached a TON of 50[60] before optimising the conditions by adding more WRCs or PPh_3 during catalysis. A supramolecular Co/Ir system reached a TON of 165 but showed low TOF since this value was reported after 15 h irradiation,[61] which is comparable with our value for **5a**. However, here the irradiation time did not exceed 8 h in our experiments. Noble metal-based systems exhibited higher TON[16,62] of up to 5000,[63] and we found that our noble metal-based WRC **8b** can clearly be enqueued with the so far developed highly efficient molecular WRCs for molecular photocatalytic water splitting, exhibiting high TONs and TOFs.

So far, several PNP complexes with different backbones and metal centres have been investigated in our group.[5,6,15,16] To highlight the positive effect of multinuclear WRCs in comparison to mononuclear species, the TONs of the most promising and structurally similar tri- and mononuclear WRCs were compared. The mononuclear complex [$Pd(ACN)_2$(PNP-C1-Me)](BF_4)$_2$, with only one palladium centre, was studied by W. Viertl *et al.*[6] The complex offered a TON of 2289 when irradiated in the presence of the same [Ir(bpy)(ppy)$_2$](PF_6) chromophore as for the analogous trinuclear complex **8b**. Although the irradiation conditions differ slightly from each other because they have been optimised in each case, the TON value is nearly four times higher with the structurally similar tris(PNP)-complex **8b** of 8899, exhibiting three metal centres. The mononuclear [$PdCl_2$(PNP-C1-Me)][6] showed a TON of 842, while the trinuclear complex **8a** exhibited a more than six times higher TON of 5154. Clearly, a beneficial cooperative effect of the multiple catalytic centres was noticed. The comparison of the mono- and trinuclear complexes and the irradiation conditions are presented in Table S6 (page 19, ESI†).

D Conclusions

Multinuclear chromophores are influenced by energy transfer processes, which were observable in the form of short excited state lifetimes and weak emissions. Therefore, the multiple PS centres hinder each other in the excited state, resulting in equal or even decreased TONs in comparison to mononuclear species.[15] The PS **4d** possessed a TON of 48 in combination with the known and benchmarked [Ni(py-S)$_3$](NEt_4) WRC and in combination with the common WRC [$Fe_3(CO)_{12}$] a TON of 37 was achieved. We found that the influence of the steric pressure of the bridging ligand backbone of the trinuclear species combined with the steric requirements of the auxiliary phenanthroline ligand is beneficial for PS reducing their non-radiative decay.

In contrast, the investigation of multinuclear WRCs and their mutual dependence displayed that multiple metal centres support the proton reduction due to the presence of more catalytically active centres. The tris($PdACN_2$)$_3$ complex **8b** showed the best results within all performed experiments, independently of the used irradiation sources. Thereby, the exchange of chloride against ACN enhanced the hydrogen production significantly. Considering the non-noble metal based complexes, the hydrogen evolution of the nickel(II) based tris-complex **7a** exhibited the best results with a TON of 460 (700 W Hg, Table 3, entry 5). The tris($CoCl_2$)$_3$ **5a** showed the

best results for the non-noble metal-based WRCs under LED irradiation (TON = 146, Table 4, entry 7). The broader and sunlight imitating spectrum of the 700 W Hg medium pressure lamp caused higher TONs (compare Tables 3 and 4); however, the turnover frequency (TOF) was enhanced extremely with the LED irradiation of the Solar Light Lab Luminaire.

Coordinatively saturated compounds like **6c**, **7a** and **9a** are certainly not the real catalysts. They are precatalysts, where the loss of a chlorido or carbonyl ligand only starts the catalysis. This has been confirmed by DFT calculations in Ref. 6. Therefore, long induction periods are typical. In Fig. 3 and 4, it is unambiguously shown that further addition of the PS restarts the catalysis. It only stops completely as soon as the WRC decomposes. This has been confirmed by ^{31}P NMR spectroscopy showing no WRC left in the final catalytic system after irradiation.

The further optimisation of the systems, for example, in the form of a water-based solvato-complex of the most promising WRC **8b** is envisioned and will probably increase the obtained TON of 8899 to even higher values. Already this TON outperforms related mononuclear catalysts and other DuBois-type WRCs.[6] ^{31}P{^{1}H} NMR results show that the molecular catalysts are destroyed as soon as the plateau for hydrogen production is reached. This is often accompanied by the observation of elemental palladium at the end of the irradiation experiments, thus confirming that this form of palladium black does not contribute to the photocatalytic hydrogen production. Since this is a reductive detrimental effect, it is clear that more sacrificial agent does not help to revive the catalyst system. Additionally, the non-noble metal-based WRCs showed promising results and could also be improved.

Conflicts of interest

There are no conflicts to declare.

Acknowledgements

We want to thank Prof. Dr Mark E. Thompson and co-workers and Prof. Dr Luisa De Cola and co-workers for electrochemical and photophysical measurements. Many thanks go to the EFRE for the financial support within the project Solar Hydrogen.

References

1 J. Barber and P. D. Tran, *J. R. Soc., Interface*, 2013, **10**, 20120984.
2 I. McConnell, G. Li and G. W. Brudvig, *Chem. Biol.*, 2010, **17**, 434–447.
3 T. M. McCormick, B. D. Calitree, A. Orchard, N. D. Kraut, F. V. Bright, M. R. Detty and R. Eisenberg, *J. Am. Chem. Soc.*, 2010, **132**, 15480–15483.
4 Y. Amao, *ChemCatChem*, 2011, **3**, 458–474.
5 C. M. Strabler, S. Sinn, R. Pehn, J. Pann, J. Dutzler, W. Viertl, J. Prock, K. Ehrmann, A. Weninger, H. Kopacka, L. de Cola and P. Brüggeller, *Faraday Discuss.*, 2017, **198**, 211–233.
6 W. Viertl, J. Pann, R. Pehn, H. Roithmeyer, M. Bendig, A. Rodríguez-Villalón, R. Bereiter, M. Heiderscheid, T. Müller, X. Zhao, T. S. Hofer, M. E. Thompson, S. Shi and P. Brueggeller, *Faraday Discuss.*, 2019, **215**, 141–161.
7 H. Fan, F. Alam, B. Hao, J. Ma, J. Zhang, Z. Ma and T. Jiang, *Theor. Chem. Acc.*, 2022, **141**, 25.
8 K. Wu and A. G. Doyle, *Nat. Chem.*, 2017, **9**, 779–784.
9 E. S. Wiedner, A. M. Appel, S. Raugei, W. J. Shaw and R. M. Bullock, *Chem. Rev.*, 2022, **122**, 12427–12474.
10 B. Pandey, J. A. Krause and H. Guan, *Inorg. Chem.*, 2022, **61**, 11143–11155.
11 X.-X. Jin, T. Li, D.-P. Shi, L.-J. Luo, Q.-Q. Su, J. Xiang, H.-B. Xu, C.-F. Leung and M.-H. Zeng, *New J. Chem.*, 2020, **44**, 13393–13400.
12 M. A. Argüello Cordero, P. J. Boden, M. Rentschler, P. di Martino-Fumo, W. Frey, Y. Yang, M. Gerhards, M. Karnahl, S. Lochbrunner and S. Tschierlei, *Inorg. Chem.*, 2022, **61**, 214–226.
13 M. Rentschler, M.-A. Schmid, W. Frey, S. Tschierlei and M. Karnahl, *Inorg. Chem.*, 2020, **59**, 14762–14771.
14 D. S. Marynick, *J. Am. Chem. Soc.*, 1984, **106**, 4064–4065.
15 J. Pann, H. Roithmeyer, W. Viertl, R. Pehn, M. Bendig, J. Dutzler, B. Kriesche and P. Brüggeller, *Sustainable Energy Fuels*, 2019, **3**, 2926–2953.
16 R. Pehn, J. Pann, K. Ehrmann, W. Viertl, H. Roithmeyer, M. Bendig, C. Strabler, H. Kopacka, T. Müller, T. Hofer and P. Brüggeller, *Eur. J. Inorg. Chem.*, 2020, 4358–4372.
17 S. Tschierlei, M. Presselt, C. Kuhnt, A. Yartsev, T. Pascher, V. Sundström, M. Karnahl, M. Schwalbe, B. Schäfer, S. Rau, M. Schmitt, B. Dietzek and J. Popp, *Chem. – Eur. J.*, 2009, **15**, 7678–7688.
18 O. J. Cooper, J. McMaster, W. Lewis, A. J. Blake and S. T. Liddle, *Dalton Trans.*, 2010, **39**, 5074.
19 M. M. Taqui Khan and B. Swamy, *Inorg. Chem.*, 1987, **26**, 178–184.
20 S. S. Rozenel, J. B. Kerr and J. Arnold, *Dalton Trans.*, 2011, **40**, 10397.
21 F. Koç, F. Michalek, L. Rumi, W. Bannwarth and R. Haag, *Synthesis*, 2005, 3362–3372.
22 J. I. van der Vlugt and J. N. H. Reek, *Angew. Chem., Int. Ed.*, 2009, **48**, 8832–8846.
23 C. A. Tolman, *Chem. Rev.*, 1977, **77**, 313–348.
24 J. Michael. Buchanan, J. M. Stryker and R. G. Bergman, *J. Am. Chem. Soc.*, 1986, **108**, 1537–1550.
25 J. Y. Yang, S. E. Smith, T. Liu, W. G. Dougherty, W. A. Hoffert, W. S. Kassel, M. R. DuBois, D. L. DuBois and R. M. Bullock, *J. Am. Chem. Soc.*, 2013, **135**, 9700–9712.
26 M. O'Hagan, W. J. Shaw, S. Raugei, S. Chen, J. Y. Yang, U. J. Kilgore, D. L. DuBois and R. M. Bullock, *J. Am. Chem. Soc.*, 2011, **133**, 14301–14312.
27 J. Pann, W. Viertl, H. Roithmeyer, R. Pehn, T. S. Hofer and P. Brüggeller, *Isr. J. Chem.*, 2022, **62**, 1–14.
28 P. Sun, D. Yang, Y. Li, B. Wang and J. Qu, *Dalton Trans.*, 2020, **49**, 2151–2158.

29 K. Koshiba, K. Yamauchi and K. Sakai, *Angew. Chem., Int. Ed.*, 2017, **56**, 4247–4251.
30 M.-H. Ho, R. Rousseau, J. A. S. Roberts, E. S. Wiedner, M. Dupuis, D. L. DuBois, R. M. Bullock and S. Raugei, *ACS Catal.*, 2015, **5**, 5436–5452.
31 Z. Han, L. Shen, W. W. Brennessel, P. L. Holland and R. Eisenberg, *J. Am. Chem. Soc.*, 2013, **135**, 14659–14669.
32 S. Roy, B. Sharma, J. Pécaut, P. Simon, M. Fontecave, P. D. Tran, E. Derat and V. Artero, *J. Am. Chem. Soc.*, 2017, **139**, 3685–3696.
33 M. Sandroni, Y. Pellegrin and F. Odobel, *C. R. Chim*, 2016, **19**, 79–93.
34 M. W. Mara, K. A. Fransted and L. X. Chen, *Coord. Chem. Rev.*, 2015, **282–283**, 2–18.
35 M. Iwamura, S. Takeuchi and T. Tahara, *Acc. Chem. Res.*, 2015, **48**, 782–791.
36 L. X. Chen, G. B. Shaw, I. Novozhilova, T. Liu, G. Jennings, K. Attenkofer, G. J. Meyer and P. Coppens, *J. Am. Chem. Soc.*, 2003, **125**, 7022–7034.
37 N. A. Gothard, M. W. Mara, J. Huang, J. M. Szarko, B. Rolczynski, J. V. Lockard and L. X. Chen, *J. Phys. Chem. A*, 2012, **116**, 1984–1992.
38 A. C. S. Samia, J. Cody, C. J. Fahrni and C. Burda, *J. Phys. Chem. B*, 2004, **108**, 563–569.
39 M. K. Eggleston, D. R. McMillin, K. S. Koenig and A. J. Pallenberg, *Inorg. Chem.*, 1997, **36**, 172–176.
40 A. Kaeser, M. Mohankumar, J. Mohanraj, F. Monti, M. Holler, J.-J. Cid, O. Moudam, I. Nierengarten, L. Karmazin-Brelot, C. Duhayon, B. Delavaux-Nicot, N. Armaroli and J.-F. Nierengarten, *Inorg. Chem.*, 2013, **52**, 12140–12151.
41 M. Rentschler, M.-A. Schmid, W. Frey, S. Tschierlei and M. Karnahl, *Inorg. Chem.*, 2020, **59**, 14762–14771.
42 M. Rentschler, S. Iglesias, M. Schmid, C. Liu, S. Tschierlei, W. Frey, X. Zhang, M. Karnahl and D. Moonshiram, *Chem. – Eur. J.*, 2020, **26**, 9527–9536.
43 R. Giereth, A. K. Mengele, W. Frey, M. Kloß, A. Steffen, M. Karnahl and S. Tschierlei, *Chem. – Eur. J.*, 2020, **26**, 2675–2684.
44 Z.-G. Niu, X.-Y. Wang, H.-H. Chen, X. Wang, S. Wei, D.-M. Wu, G.-Y. Chen, J. Qin and G.-N. Li, *Acta Chim. Slov.*, 2017, 633–637.
45 V. Balzani, A. Credi and M. Venturi, *Nano Today*, 2007, **2**, 18–25.
46 H. Roithmeyer, J. Pann, M. Bendig, R. Bereiter,., E. Ladstätter, R. Pehn, J. Prock, W. Viertl and P. Brüggeller, *Polyhedron*, 2018, **140**, 78–83.
47 P. Jarosz, J. Thall, J. Schneider, D. Kumaresan, R. Schmehl and R. Eisenberg, *Energy Environ. Sci.*, 2008, **1**, 573.
48 M. Taniguchi and J. S. Lindsey, *Tetrahedron*, 2010, **66**, 5549–5565.
49 M. Herder, F. Eisenreich, A. Bonasera, A. Grafl, L. Grubert, M. Pätzel, J. Schwarz and S. Hecht, *Chem. – Eur. J.*, 2017, **23**, 3743–3754.
50 S. Fischer, D. Hollmann, S. Tschierlei, M. Karnahl, N. Rockstroh, E. Barsch, P. Schwarzbach, S.-P. Luo, H. Junge, M. Beller, S. Lochbrunner, R. Ludwig and A. Brückner, *ACS Catal.*, 2014, **4**, 1845–1849.
51 E. Mejía, S.-P. Luo, M. Karnahl, A. Friedrich, S. Tschierlei, A.-E. Surkus, H. Junge, S. Gladiali, S. Lochbrunner and M. Beller, *Chem. – Eur. J.*, 2013, **19**, 15972–15978.
52 X. Feng, Y. Pi, Y. Song, C. Brzezinski, Z. Xu, Z. Li and W. Lin, *J. Am. Chem. Soc.*, 2020, **142**, 690–695.
53 Q.-F. Chen, Z.-Y. Cheng, R.-Z. Liao and M.-T. Zhang, *J. Am. Chem. Soc.*, 2021, **143**, 19761–19768.
54 T. Zhang, C. Wang, S. Liu, J.-L. Wang and W. Lin, *J. Am. Chem. Soc.*, 2014, **136**, 273–281.
55 H. Yuan, B. Cheng, J. Lei, L. Jiang and Z. Han, *Nat. Commun.*, 2021, **12**, 1835.
56 P. Delahay and C. T. Fike, *J. Am. Chem. Soc.*, 1958, **80**, 2628–2630.
57 S. G. Mairanovskii, *Catalytic and Kinetic Waves in Polarography*, Springer, US, Boston, MA, 1968.
58 A. D. Wilson, R. K. Shoemaker, A. Miedaner, J. T. Muckerman, D. L. DuBois and M. R. DuBois, *Proc. Natl. Acad. Sci. U. S. A.*, 2007, **104**, 6951–6956.
59 B. Probst, M. Guttentag, A. Rodenberg, P. Hamm and R. Alberto, *Inorg. Chem.*, 2011, **50**, 3404–3412.
60 P. Zhang, P.-A. Jacques, M. Chavarot-Kerlidou, M. Wang, L. Sun, M. Fontecave and V. Artero, *Inorg. Chem.*, 2012, **51**, 2115–2120.
61 A. Fihri, V. Artero, A. Pereira and M. Fontecave, *Dalton Trans.*, 2008, 5567.
62 J. Pann, K. Ehrmann, R. Pehn, H. Roithmeyer, W. Viertl, H. Kopacka, P. Brüggeller and W. Oberhauser, *Inorg. Chim. Acta*, 2021, **516**, 120162.
63 E. D. Cline, S. E. Adamson and S. Bernhard, *Inorg. Chem.*, 2008, **47**, 10378–10388.